Energetics, equation of state, and elasticity of NAL phase: Potential host for alkali and aluminum in the lower mantle

Mainak Mookherjee,[1] Bijay B. Karki,[2] Lars Stixrude,[3] and Carolina Lithgow-Bertelloni[3]

Received 24 August 2012; accepted 5 September 2012; published 12 October 2012.

[1] The new aluminous (NAL) phase and aluminous phase with calcium ferrite (CF) structure constitutes more than 25 volume % of the deeply subducted crust at lower mantle depths. Using first principle simulations, we calculate the energetics, equation of state, and elasticity of NAL phase with a widely varying composition including $CaMg_2Al_6O_{12}$, $NaNa_2Al_3Si_3O_{12}$ and $KNa_2Al_3Si_3O_{12}$. Our calculations indicate the relative stability of NAL and CF phases is a sensitive function of pressure, temperature, and composition, with increasing pressure tending to favor the CF phase, and increasing temperature, Mg-content and alkali-content tending to favor the NAL phase. The sound wave velocities of the NAL phase is significantly lower than CF phases and other major lower mantle phases. In deeply subducted MORB and CC, the faster sound velocity of silica (SiO_2) and its high-pressure polymorphic phase is likely to be compensated with the slower sound wave velocities of NAL phase. **Citation:** Mookherjee, M., B. B. Karki, L. Stixrude, and C. Lithgow-Bertelloni (2012), Energetics, equation of state, and elasticity of NAL phase: Potential host for alkali and aluminum in the lower mantle, *Geophys. Res. Lett.*, *39*, L19306, doi:10.1029/2012GL053682.

1. Introduction

[2] Subducted crust has a distinct major and trace element chemistry in comparison to peridotites. While the bulk silicate Earth contains 4.5 wt% alumina [*McDonough and Sun*, 1995], oceanic (MORB) and continental crust (CC) are significantly enriched with ~15–16 wt% alumina [*Irifune and Ringwood*, 1993; *Kesson et al.*, 1994], while subducted terrigenous sediments may have alumina content of 20 wt% [*Irifune et al.*, 1994]. This high alumina content stabilizes aluminous phases in deeply subducted crust that are not present in mantle peridotite. At lower mantle depths, the volume fraction of the CF and NAL phases in MORB is ~10–25 vol% [*Ricolleau et al.*, 2010] (Figure 1). NAL may also be stabilized in deeply subducted Archean continental crust (CC) of tonalite-trondjhemite-granodiorite (TTG) composition [*Kawai et al.*, 2009; *Komabayashi et al.*, 2009]. Moreover, the NAL and CF phases are known to host the alkali elements (Na and K) that are enriched in subducted crust as compared with average mantle [*Miyajima et al.*, 2001].

[3] Despite their importance in understanding the buoyancy of subducted crust and its possible accumulation at the base of the mantle [*Ricolleau et al.*, 2010], and its seismic detectability, little is known of the physical properties of the aluminous phases compared with those stable in peridotite. The seismic wave velocities of the NAL and CF phases are unknown at lower mantle conditions, and the density is known in only a few bulk compositions. Moreover, the factors governing the relative stability of CF and NAL phases are poorly understood. Which of these phases is stable, and over what range of pressure, temperature, and bulk composition, may be important because they are likely to have distinct physical properties. One of the challenges in understanding these phases is that they exhibit a wide range of compositions incorporating alkali and alkaline earth elements as well as Al and Si.

[4] In this article, we explore the relative stability of NAL and CF phases and compare their physical properties, including density and seismic wave velocities in order to evaluate their role in subducted crustal buoyancy and the detectability of deeply subducted crust. We compute the enthalpy, equation of state, and full elastic constant tensor across a wide range of plausible mantle compositions along the $Na_3Al_3Si_3O_{12}$-$K_3Al_3Si_3O_{12}$ and $Ca_3Al_6O_{12}$-$Mg_3Al_6O_{12}$ joins. Computations of equation of state and elasticity focus on the NAL phase, which we compare with our previous calculations of these quantities in the CF phase [*Mookherjee*, 2011].

2. Method

[5] The NAL phase has a hexagonal space group $P6_3/m$ [*Miura et al.*, 2000] and a structural formula of $A^{IX}B_2^{VIII}C_6^{VI}O_{12}$. The A^{IX} site is a nine-fold coordinated tunnel with a hexagonal cross-section and is typically occupied by a large monovalent (e.g., Na^+, K^+) or divalent cation (e.g., Ca^{2+}). The cation in the A^{IX} site is likely to be disordered owing to its Wyckoff symmetry being 2a and only one atom occupies either of the two equivalent sites, i.e., half occupancy. The B^{VIII} site has a di-trigonal cross section and is typically occupied by a smaller cation (e.g., Mg^{2+}, Fe^{2+}). The C^{VI} site is octahedral site and is typically occupied by a framework-forming cation (e.g., Al^{3+}, Si^{4+}). The octahedral units form edge-sharing double chains in the hexagonal aluminous phase (Figure 1). The structural formula of the CF phase may be written in a 12 oxygen basis to permit direct comparison with that of the NAL phase: $B_3^{VIII}C_6^{VI}O_{12}$ with an orthorhombic space group (*Pbnm*) and four formula units (Z = 4 on a 4 O primitive basis) in the unit cell [*Decker and Kasper*, 1957]. The B^{VIII} sites are often occupied by Na^{1+}, Mg^{2+} or Ca^{2+} cations whereas the C^{VI} sites are typically a framework-forming cation (e.g., Al^{3+}, Si^{4+}) similar to the NAL phases (Figure 1).

[1]Department of Earth and Atmospheric Sciences, Cornell University, Ithaca, New York, USA.
[2]Department of Computer Sciences and Department of Geology and Geophysics, Louisiana State University, Baton Rouge, Louisiana, USA.
[3]Department of Earth Sciences, University College London, London, UK.

Corresponding author: M. Mookherjee, Department of Earth and Atmospheric Sciences, Cornell University, Ithaca, NY 14850, USA. (mm2457@cornell.edu)

0094-8276/12/2012GL053682

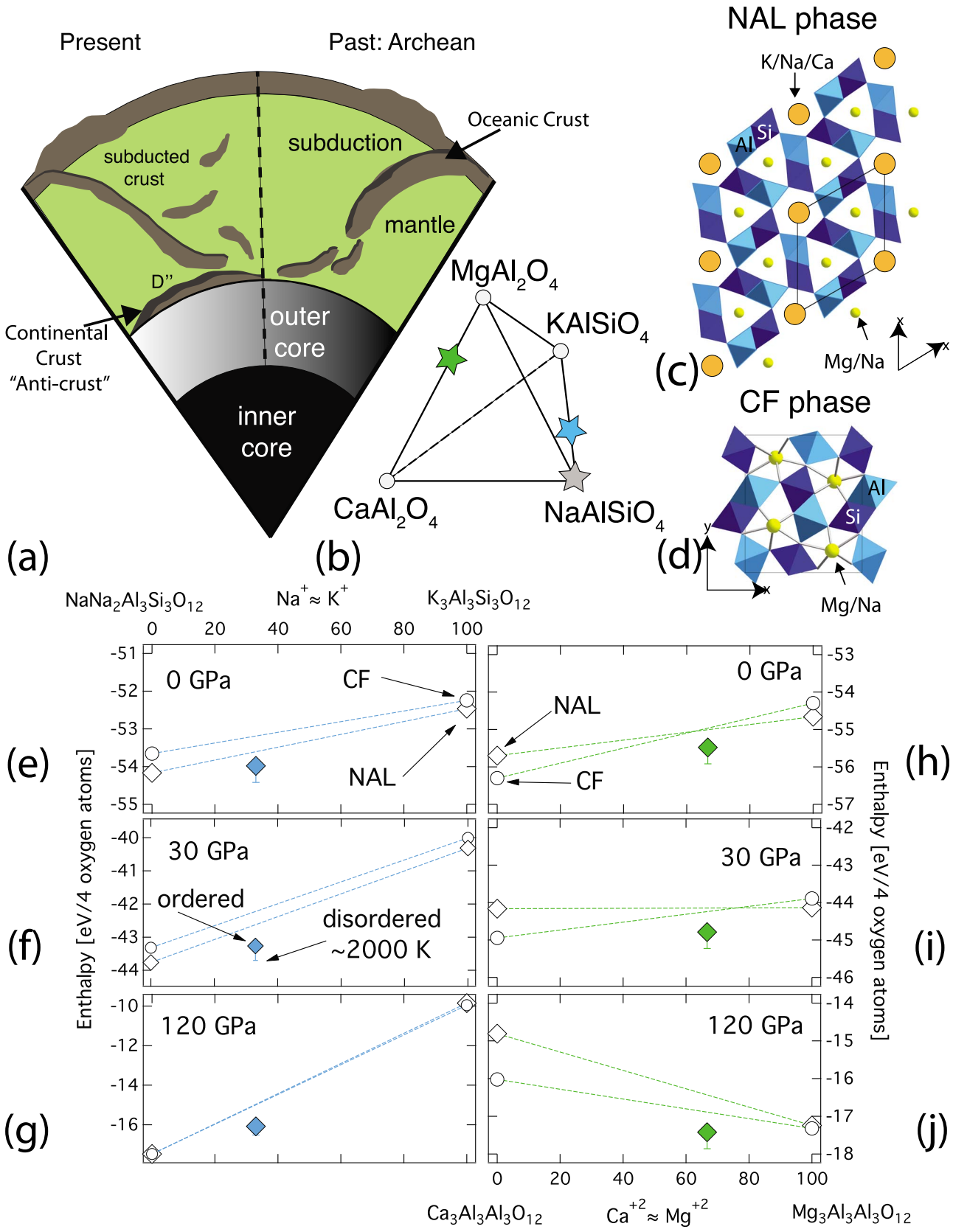
Present
Past: Archean
subducted crust
subduction
Oceanic Crust
mantle
D''
outer core
inner core
Continental Crust "Anti-crust"
(a)
MgAl2O4
KAlSiO4
CaAl2O4
NaAlSiO4
(b)
NAL phase
K/Na/Ca
Si
Al
Mg/Na
(c)
CF phase
Al
Si
Mg/Na
(d)
NaNa2Al3Si3O12
Na+≈ K+
K3Al3Si3O12
0 GPa
CF
NAL
(e)
0 GPa
NAL
CF
(h)
30 GPa
ordered
disordered ~2000 K
(f)
30 GPa
(i)
120 GPa
(g)
120 GPa
(j)
Enthalpy [eV/4 oxygen atoms]
Ca3Al3Al3O12
Ca+2≈ Mg+2
Mg3Al3Al3O12

Figure 1

[6] Static, density functional theory calculations (VASP) were performed with the local density approximation (LDA) and ultrasoft pseudopotentials as described in *Mookherjee and Steinle-Neumann* [2009a, 2009b] and *Mookherjee* [2011]. Calculations for NAL phase are performed in a 21 atom primitive unit cell, and for the CF phases a 28 atom primitive unit cell. We consider the following compositions for both phases: $Ca_3Al_6O_{12}$, $Mg_3Al_6O_{12}$, $Na_3(Al_3Si_3)O_{12}$, $K_3(Al_3Si_3)O_{12}$ and for the more flexible NAL phase only the intermediate compositions: $CaMg_2Al_6O_{12}$, $KNa_2(Al_3Si_3)O12$ and $NaNa_2(Al_3Si_3)O_{12}$. We use an energy cutoff E_{cut} = 600 eV and k-point mesh of $2 \times 2 \times 2$. A series of convergence tests demonstrated that these computational parameters yield total energies that are converged to within 10 meV/atom. We analyze bulk compression behavior using the third order-Birch Murnaghan equation-of-state [*Birch*, 1978]. Full elastic constant tensor were determined by straining the lattice by 1%, the details of the methods are described in [*Karki et al.*, 2001]. Four distinct strain tensors $\underline{\underline{\varepsilon}}$ are applied to calculate the five elastic constants C_{11}, C_{12}, C_{13}, C_{33}, and C_{44} of hexagonal symmetry. Finite strain fits to the elasticity data were made using the finite strain formulations as in our previous studies [*Karki et al.*, 2001; *Mookherjee et al.*, 2011]. We computed the single crystal azimuthal anisotropy for P- and S-waves using the formulation for maximum polarization anisotropy [*Mainprice*, 1990].

3. Results

[7] Our calculations reveal that with increasing pressure, the enthalpy of the CF phase lowers with respect to the NAL phase for all compositions. This trend explains the disappearance of NAL from the MORB compositions at pressures ~40 GPa [*Ricolleau et al.*, 2010]. On the alkali (K-Na) join NAL remains more stable than CF even at core-mantle boundary pressure. This emphasizes that the large ions are readily accommodated in the NAL structure, which unlike the CF structure, features a nine-fold coordinated site. There is excellent agreement between our predicted energetics and the experimental phase diagram along the $Ca_3Al_6O_{12}$-$Mg_3Al_6O_{12}$ join [*Akaogi et al.*, 1999] including the stability of NAL at the $Mg_3Al_6O_{12}$-end, the CF phase at the $Ca_3Al_6O_{12}$-end, and the field of pure NAL at $CaMg_2Al_6O_{12}$ composition at all pressures up to CMB, with the 1:2 Ca:Mg ratio accommodated by the 1:2 ratio of nine- to eight-fold coordinated sites in the NAL structure (Figure 1).

[8] The equation of state of the NAL phase is well represented by a third order Birch-Murnaghan formulation (Figure 2 and Table 1). The theoretical results are in good agreement with the experimentally observed and theoretically determined compressibilities for NAL phase [*Vanpeteghem et al.*, 2003; *Guignot and Andrault*, 2004; *Kawai and Tsuchiya*, 2012].

[9] The elastic constants of the NAL phase increase monotonically with pressure up to lower mantle pressure for all phases and compositions, demonstrating mechanical stability (Figure 2). The C_{33} elastic modulus is always stiffer than C_{11} at all pressures and in all compositions. The maximum stiffness along *c*-axes is related to the sharing of edges by the stiff octahedral units along the channel direction (Figure 1). In the direction perpendicular to the channel, these polyhedra share corners and the compression is accommodated by adjusting the Si(Al)-O-Si(Al) hinge angles and di-trigonal shape of the channels. The shear elastic modulus C_{44} is the softest compared to the principal and off-diagonal elastic modulus (Figure 2).

[10] The elasticity of the aluminous phases are sensitive to the chemistry and the crystal structure, i.e., NAL *vs.* CF phase (Figure 3 and Table 2). The S-wave velocity of the NAL phase is substantially less than that of the CF phase in alkali- (Na-K) and alkaline-earth (Ca-Mg) compositions. In both phases, alkaline-earth compositions are faster than alkali compositions when compared at the same density, consistent with the greater compressibility of alkali cations as compared with alkaline-earth cations [*Hazen and Finger*, 1979]. The elastic anisotropy also depends on chemistry and crystal structure (Figure 3). At the upper part of the lower mantle the anisotropy of the CF phase [*Mookherjee*, 2011] is larger than the NAL phase (Figure 3). At higher pressure, A_P and A_{S1} anisotropy significantly reduces, whereas A_{S2} increases.

4. Geophysical Implications

[11] Our results indicate that the relative stability of the NAL and CF phases is a sensitive function of pressure, temperature, and composition. While pressure tends to favor stability of the CF phase, enrichment in Mg or alkalis tends to favor the NAL phase. We anticipate the range of stability of the NAL phase in the lower mantle will be a sensitive function of composition, particularly of the whole-rock Mg and alkali concentrations. Previous experimental results on one particular basalt composition, which shows the NAL phase stable to about 40 GPa [*Ricolleau et al.*, 2010], may not be representative of all geophysically relevant basalts, and variations in alkali or Mg content, due for example to processing of subducted oceanic crust on its way down through the arc, or differing conditions of oceanic crust

Figure 1. (a) Schematic diagram illustrating mantle heterogeneity consisting of fragments of subducted oceanic crusts. The recycled oceanic crust, through subduction, is the primary source of heterogeneity in the mantle [*Brandenburg and van Keken*, 2007; *Nakagawa et al.*, 2010]. It is likely that the subducted crusts might have accumulated at the CMB over geological times [*Kawai et al.*, 2009; *Komabayashi et al.*, 2009]. (b) A tetrahedral plot showing the various end-member composition of the aluminous phase. In this study we have considered, NAL phases with $KNa_2Al_3Si_3O_{12}$ (light blue star); $NaNa_2Al_3Si_30_{12}$ (grey star) and $CaMg_2Al_6O_{12}$ (green star) stoichiometry; crystal structure of (c) NAL phase and (d) CF phase. The energetics along $NaAlSiO_4$-$KAlSiO_4$ join (e) at 0 GPa, (f) at 30 GPa, and (g) at 120 GPa; the blue filled rhomb represents the NAL phase with $KNa_2Al_3SiO_{12}$ stoichiometry; the end members, open circles- CF phase; open rhombs NAL phase. The energetics along $CaAl_2O_4$-$MgAl_2O_4$ join is shown in (h) at 0 GPa, (i) at 30 GPa, and (j) at 120 GPa; the green filled rhomb represents $CaMg_2Al_6O_{12}$ stoichiometry with hexagonal symmetry; the end members, open circles- CF phase; open rhombs NAL phase. The relative magnitude of $-TS_{config}$ term for complete disorder configuration of K and Na atom in $KNa_2Al_3Si_3O_{12}$ and Ca and Mg in $CaMg_2Al_6O_{12}$ is also shown at T = 2000 K.

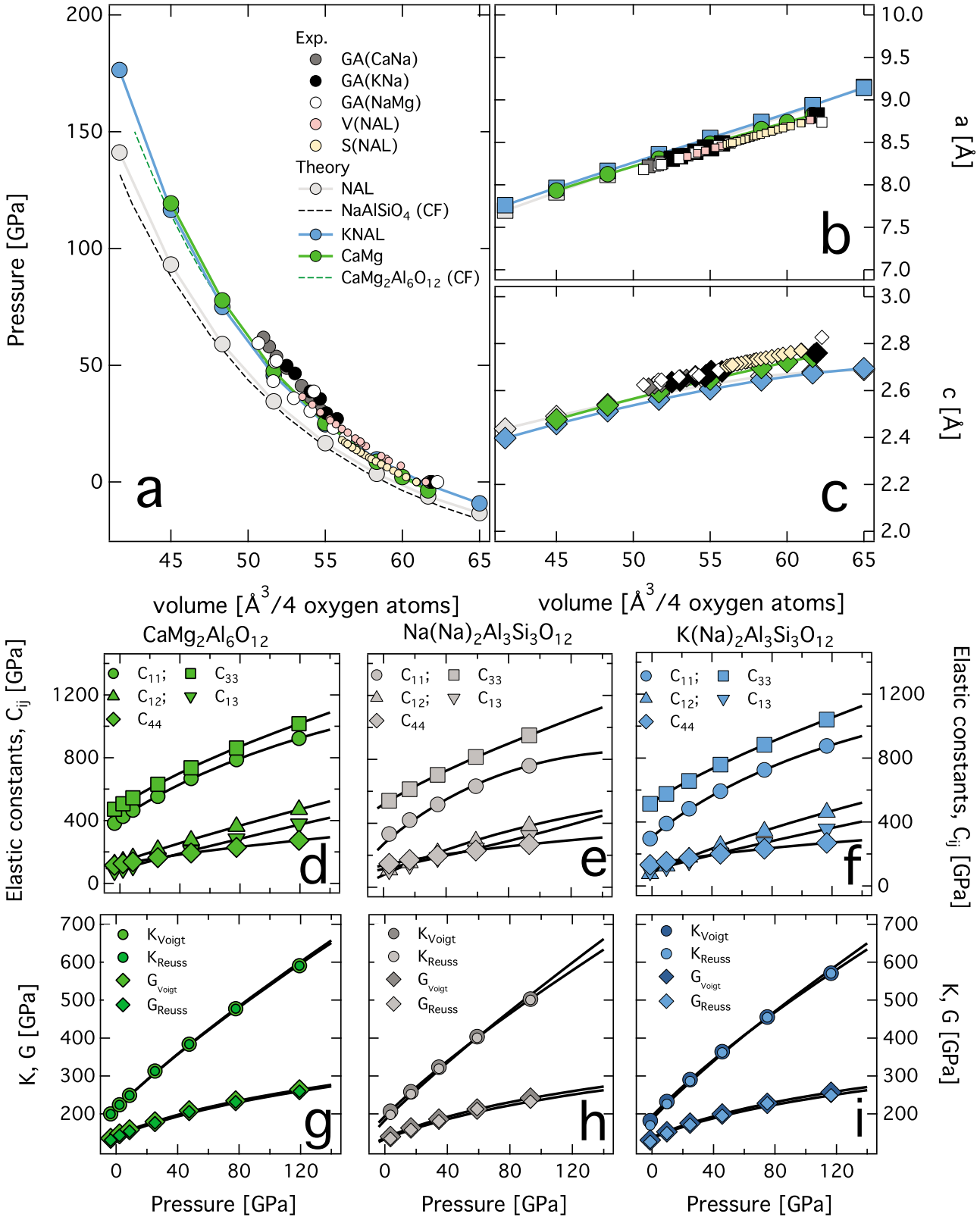

Figure 2. (a) Equation of state (pressure-volume plot) for NAL phases and CF phases with $NaAlSiO_4$ [*Mookherjee*, 2011] and $CaMg_2Al_6O_{12}$ stoichiometry. The $CaMg_2Al_6O_{12}$ stoichiometry is derived from [(1/3) $CaAl_2O_4$ + (2/3) $MgAl_2O_4$]. (b) Lattice parameter- *a*; and (c) *c* vs. unit-cell volume; experimental data are from GA: [*Guignot and Andrault*, 2004]; V: [*Vanpeteghem et al.*, 2003] and S: [*Shinmei et al.*, 2005]; calculations, NAL refers to $NaNa_2Al_3Si_3O_{12}$; KNAL refers to $KNa_2Al_3Si_3O_{12}$ and CaMg refers to $CaMg_2Al_6O_{12}$; Calculated elastic constants: (d–f) longitudinal elastic constants C_{11}; C_{33}, off-diagonal elastic constants C_{12} and C_{13} and shear elastic constants C_{44}; (g–i) Bulk (*K*) and shear (*G*) moduli for the NAL phases considered in this study. Lines are finite strain fits with the parameters listed in (Table 2).

Table 1. Equation of State Parameter for NAL and CF Phases[a]

Chemistry	V_0	K_0	K'	References
		NAL Phase		
$(Na)(Na)_2Al_3Si_3O_{12}$	178.3 (59.4)	185	4.0	LDA [this study]
$(K)(Na)_2Al_3Si_3O_{12}$	183.7 (61.2)	177	4.9	
$(K)(K)_2Al_3Si_3O_{12}$	210.7 (70.2)	147	4.8	
$(Mg)(Mg)_2Al_6O_{12}$	179.1 (59.7)	211	4.0	
$(Ca)(Mg)_2Al_6O_{12}$	181.8 (60.6)	212	4.2	
$(Ca)(Ca)_2Al_6O_{12}$	196.8 (65.6)	199	4.2	
		CF Phase		
$(Na)_3Al_3Si_3O_{12}$[b]	235.4 (58.9)	195	4.0	
$(K)_3Al_3Si_3O_{12}$[b]	284.0 (71.0)	130	4.0	
$(Mg)_3(Al_3Al_3)O_{12}$[b]	235.9 (59.0)	213	3.8	
$(Ca)_3(Al_3Al_3)O_{12}$[b]	258.5 (64.6)	196	4.3	
		Experiments		
Na, Mg rich	188.0 (62.7)	184	4.0	*Guignot and Andrault* [2004]
Ca, Na rich	185.3 (61.8)	177	6.5	
Ca, Na rich	184.2 (61.4)	226	4.0	
K rich	186.4 (62.1)	183	5.8	
K rich	185.8 (61.9)	217	4.0	
Na, Mg rich	184.6 (61.5)	214	3.0	*Vanpeteghem et al.* [2003]
		Ab Inito		
$NaAlSiO_4$	176.1 (58.7)	197	4.5	*Kawai and Tsuchiya* [2012]

[a]Unit of volume (V_0) and bulk modulus (K_0) are $Å^3$ and GPa respectively.
[b]Stoichiometry expressed in 12 oxygen basis; in brackets, we report the V_0 for 4 oxygen atom basis.

formation in the early earth may lead to differing extents of NAL stability. Stability of NAL in continental crustal compositions likely also depends on the bulk composition, e.g. present day mean CC vs. TTG compositions that may have been more important in the past [*Komabayashi et al.*, 2009].

[12] The relative stability of NAL and CF phases is important because as shown by our results, they have distinctive physical properties. The NAL phase is seismically slower than the CF phase. Thus any attempt to draw conclusions about the seismic signature of deeply subducted crust, or possible large-scale ponding of ancient crust at the base of the mantle, must account for the relative stability of these two phases. Stability of the NAL phase in the deep lower mantle may be particularly important for understanding the origin of large-scale low velocity provinces [*Garnero and McNamara*, 2008]. Our results indicate that previous attempts to model the seismic signature of subducted crust need to be modified to account for the possibly stability of NAL. In the study of [*Ricard et al.*, 2005], excess alumina in subducted crust was modeled as pure Al_2O_3 (and high pressure polymorphs) phase. This is incorrect since based on phase relations it is known that crustal compositions stabilize CF and NAL phases, and CF and NAL are much slower than pure Al_2O_3 compounds (Figure 3). Recent studies on seismic profiles of MORB have incorporated CF phases [*Xu et al.*, 2008] as a proxy for the entire suite of possible aluminous phase in subducted crust. This requires further revisions since our study indicates that (a) chemistry (large incompatible cations) dictates the relative stability of NAL and CF phase; and (b) NAL has very low seismic velocity compared with CF.

Figure 3. Velocity density systematics: (a) compressional and (b) shear wave velocities, the solid black lines represents the linear relation for constant mean atomic weights; the thick grey line represents PREM [*Dziewonski and Anderson*, 1981]. The velocities of major mantle phases - $MgSiO_3$ perovskite, MgO, $CaSiO_3$ perovskite, SiO_2 and Al_2O_3 are from [*Karki et al.*, 2001]. Two aluminous phases ($NaAlSiO_4$ and $MgAl_2O_4$) with CF structure are from [*Mookherjee*, 2011]; the grey; blue and green filled circles represents NAL phase with $NaNa_2Al_3Si_3O_{12}$, $KNa_2Al_3Si_3O_{12}$ and $CaMg_2Al_6O_{12}$ stoichiometry from this study; (c) dependence of P-wave; (d) S1- and S2- wave velocities with direction at $V \sim 155$ $Å^3$ for NAL phases; (e) variation of A_P; (f) A_{S1} and A_{S2} anisotropy with pressure.

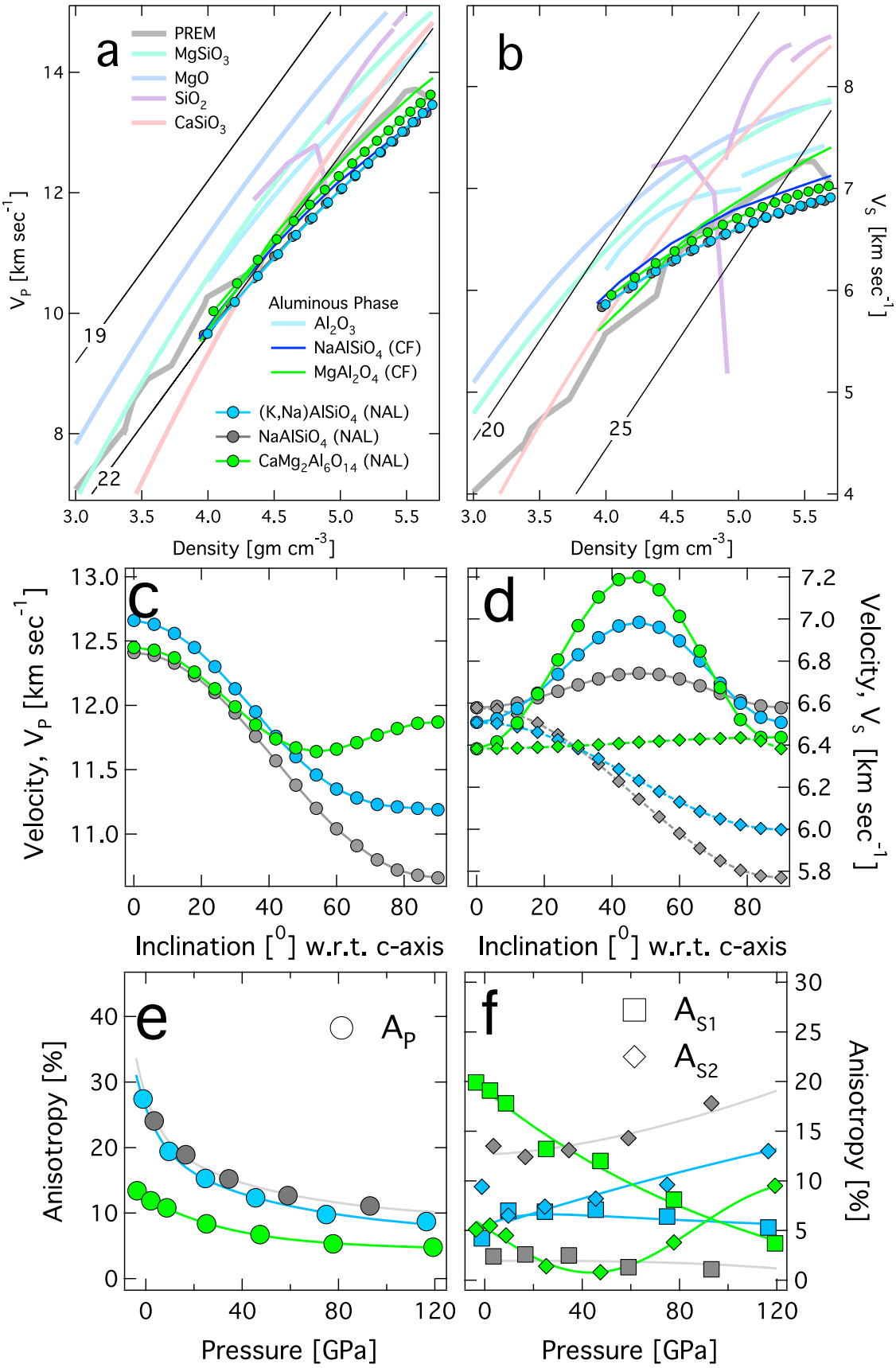
a
PREM
MgSiO3
MgO
SiO2
CaSiO3
Aluminous Phase
Al2O3
NaAlSiO4 (CF)
MgAl2O4 (CF)
(K,Na)AlSiO4 (NAL)
NaAlSiO4 (NAL)
CaMg2Al6O14 (NAL)
19
22
VP [km sec-1]
Density [gm cm-3]
b
20
25
VS [km sec-1]
Density [gm cm-3]
c
Velocity, VP [km sec-1]
Inclination [0] w.r.t. c-axis
d
Velocity, VS [km sec-1]
Inclination [0] w.r.t. c-axis
e
AP
Anisotropy [%]
Pressure [GPa]
f
AS1
AS2
Anisotropy [%]
Pressure [GPa]

Figure 3

Table 2. Elastic Constants (C_{ij}), and Bulk (K) and Shear (G) Moduli for NAL Phase[a]

V	P	C_{11}	C_{12}	C_{13}	C_{33}	C_{44}	K_{Voigt}	K_{Reuss}	G_{Voigt}	G_{Reuss}
					$KNa_2Al_3Si_3O_{12}$					
195	−9	202	41	71	467	113	138	116	107	99
185	−1	296	77	94	515	132	182	170	131	126
175	10	390	125	121	576	151	232	226	153	149
165	25	483	180	157	657	175	290	286	176	172
155	46	593	253	206	759	201	364	362	200	195
145	75	726	342	270	883	232	455	455	228	228
135	117	876	461	356	1041	269	571	571	257	249
125	176	1073	616	471	1244	316	723	723	294	282
					Finite Strain Fit					
184	0	307	82	98	522	134	194	186	138	136
		8.0[b]	4.3	2.7	6.4	1.9	3.9	4.1	1.7	1.6
					$NaNa_2Al_3Si_3O_{12}$					
195	−14	118	−3	87	454	107	115	55	90	71
185	−6	213	48	111	463	125	159	130	108	100
175	4	333	108	109	541	147	207	198	140	135
165	17	420	153	142	613	171	258	252	163	158
155	34	518	215	185	703	197	323	319	186	181
145	58	632	289	244	815	229	404	401	213	213
135	90	760	384	322	950	269	503	501	241	233
125	134	925	504	428	1122	319	633	631	277	265
					Finite Strain Fit					
178	0	270	77	114	520	138	194	183	137	133
		8.9[b]	4.6	2.0	6.2	2.1	3.8	4.1	1.7	1.6
					$CaMg_2Al_6O_{12}$					
185	−4	382	472	124	79	115	200	200	136	131
180	2	426	506	142	94	126	224	224	147	143
175	9	466	545	163	110	137	249	249	158	154
165	25	554	631	216	162	164	313	313	179	176
155	47	668	735	275	208	193	384	384	209	205
145	78	787	862	362	284	229	477	477	235	232
135	119	923	1017	470	379	274	591	591	264	259
					Finite Strain Fit					
182	0	410	135	88	494	122	216	216	145	141
		6.5[b]	3.3	2.7	6.0	1.8	3.8	3.8	1.6	1.6

[a]Pressure (P) and elastic moduli (C_{ij}, K and G) are in GPa and volume (V) is in Å^3.
[b]Pressure derivatives, $\partial M/\partial P$, where M refers to C_{ij}; K and G.

[13] **Acknowledgment.** The Editor thanks the anonymous reviewers. Authors acknowledge constructive criticism by two anonymous reviewers.

References

Akaogi, M., et al. (1999), High pressure transitions in the system $MgAl_2O_4$–$CaAl_2O_4$: New hexagonal aluminous phase with implication for the lower mantle, *Phys. Earth Planet. Inter.*, *115*, 67–77, doi:10.1016/S0031-9201(99)00076-X.

Birch, F. (1978), Finite strain isotherm and velocities for single crystal and polycrystalline NaCl at high-pressures and 300 K, *J. Geophys. Res.*, *83*, 1257–1268, doi:10.1029/JB083iB03p01257.

Brandenburg, J. P., and P. E. van Keken (2007), Deep storage of oceanic crust in a vigorously convecting mantle, *J. Geophys. Res.*, *112*, B06403, doi:10.1029/2006JB004813.

Decker, B. F., and J. S. Kasper (1957), The structure of calcium ferrite, *Acta Crystallogr., Sect. B Struct. Sci.*, *42*, 229–236.

Dziewonski, A. M., and D. L. Anderson (1981), Preliminary reference Earth model, *Phys. Earth Planet. Inter.*, *25*, 297–356, doi:10.1016/0031-9201(81)90046-7.

Garnero, E. J., and A. K. McNamara (2008), Structure and dynamics of Earth's lower mantle, *Science*, *320*, 626–628, doi:10.1126/science.1148028.

Guignot, N., and D. Andrault (2004), Equations of state of Na-K-Al host phases and implications for MORB density in the lower mantle, *Phys. Earth Planet. Inter.*, *143-144*, 107–128, doi:10.1016/j.pepi.2003.09.014.

Hazen, R. M., and L. W. Finger (1979), Bulk modulus-volume relationship for cation-anion polyhedral, *J. Geophys. Res.*, *84*, 6723–6728, doi:10.1029/JB084iB12p06723.

Irifune, T., and A. E. Ringwood (1993), Phase transformations in subducted oceanic crust and buoyancy relationships at depths of 600–800 km in the mantle, *Earth Planet. Sci. Lett.*, *117*, 101–110, doi:10.1016/0012-821X(93)90120-X.

Irifune, T., et al. (1994), Subduction of continental crust and terrigenous and pelagic sediments: An experimental study, *Earth Planet. Sci. Lett.*, *126*, 351–368, doi:10.1016/0012-821X(94)90117-1.

Karki, B. B., et al. (2001), High-pressure elastic properties of major materials of Earth's mantle from first principles, *Rev. Geophys.*, *39*, 507–534, doi:10.1029/2000RG000088.

Kawai, K., and T. Tsuchiya (2012), Phase stability and elastic properties of the NAL and CF phases in the $NaMg_2Al_5SiO_{12}$ system from first principles, *Am. Mineral.*, *97*, 305–314, doi:10.2138/am.2012.3915.

Kawai, K., et al. (2009), Lost primodial continents, *Gondwana Res.*, *16*, 581–586.

Kesson, S. E., et al. (1994), Mineral chemistry and density of subducted basaltic crust at lower mantle pressures, *Nature*, *374*, 243–245.

Komabayashi, T., et al. (2009), A speculation on the structure of the D″ layer: The growth of anti-crust at the core-mantle boundary through subduction history of the Earth, *Gondwana Res.*, *15*, 342–353.

Mainprice, D. (1990), A Fortran program to calculate seismic anisotropy from the lattice preferred orientation of minerals, *Comput. Geosci.*, *16*, 385–393, doi:10.1016/0098-3004(90)90072-2.

McDonough, W. F., and S.-S. Sun (1995), The composition of the Earth, *Chem. Geol.*, *120*, 223–253, doi:10.1016/0009-2541(94)00140-4.

Miura, H., et al. (2000), Crystal structure of $CaMg_2Al_6O_{12}$, a new Al-rich high pressure form, *Am. Mineral.*, *85*, 1799–1803.

Miyajima, M., et al. (2001), Potential host phase of aluminum and potassium in the Earth's lower mantle, *Am. Mineral.*, *86*, 740–746.

Mookherjee, M. (2011), Mid-mantle anisotropy: Elasticity of aluminous phase in subducted MORB, *Geophys. Res. Lett.*, *38*, L14302, doi:10.1029/2011GL047923.

Mookherjee, M., and G. Steinle-Neumann (2009a), Detecting deeply subducted crust from the elasticity of hollandite, *Earth Planet. Sci. Lett.*, *288*, 349–358, doi:10.1016/j.epsl.2009.09.037.

Mookherjee, M., and G. Steinle-Neumann (2009b), Elasticity of phase-X at high pressure, *Geophys. Res. Lett.*, *36*, L08307, doi:10.1029/2009GL037782.

Mookherjee, M., et al. (2011), High-pressure behavior of iron carbide (Fe_7C_3) at inner core conditions, *J. Geophys. Res.*, *116*, B04201, doi:10.1029/2010JB007819.

Nakagawa, T., et al. (2010), The influence of MORB and harzburgite composition on thermo-chemical mantle convection in a 3-D spherical shell with self-consistently calculated mineral physics, *Earth Planet. Sci. Lett.*, *296*, 403–412, doi:10.1016/j.epsl.2010.05.026.

Ricard, Y., et al. (2005), Synthetic tomographic images of slabs from mineral physics, in *Earth's Deep Mantle: Structure, Composition, and Evolution*, *Geophys. Monogr. Ser*, vol. 160, edited by R. D. van der Hilst et al., pp. 283–300, AGU, Washington, D. C., doi:10.1029/160GM17.

Ricolleau, A., et al. (2010), Phase relations and equation of state of a natural MORB: Implications for the density profile of subducted oceanic crust in the Earth's lower mantle, *J. Geophys. Res.*, *115*, B08202, doi:10.1029/2009JB006709.

Shinmei, T., et al. (2005), High-temperature and high-pressure equation of state for the hexagonal phase in the system $NaAlSiO_4$-$MgAl_2O_4$, *Phys. Chem. Miner.*, *32*, 594–602, doi:10.1007/s00269-005-0029-y.

Vanpeteghem, C. B., et al. (2003), The compressibility of hexagonal Al-rich NAL phase: similarities and differences with calcium ferrite-type (CF) phase with implications for the lower mantle, *Phys. Earth Planet. Inter.*, *138*, 223–230, doi:10.1016/S0031-9201(03)00155-9.

Xu, W., et al. (2008), The effect of bulk composition and temperature on mantle seismic structure, *Earth Planet. Sci. Lett.*, *275*, 70–79, doi:10.1016/j.epsl.2008.08.012.